The Astrophysical Journal Letters, 905:L5 (6pp), 2020 December 10 https://doi.org/10.3847/2041-8213/abca32

Application of The Wind-driven Model to a Sample of Tidal Disruption Events

Kohki Uno and Keiichi Maeda
Department of Astronomy, Kyoto University, Kitashirakawa-Oiwake-cho, Sakyo-ku, Kyoto, 606-8502, Japan; k.uno@kusastro.kyoto-u.ac.jp
Received 2020 September 8; revised 2020 October 26; accepted 2020 November 13; published 2020 December 8

Abstract

An origin of the optical/ultraviolet (UV) radiation from tidal disruption events (TDEs) has recently been discussed for different scenarios, but observational support is generally lacking. In this Letter, we test the applicability of the "wind-driven model" for a sample of UV/optical TDEs. With the model, we aim to derive the physical properties of the optical/UV TDEs, such as mass-loss rates and characteristic radii. The model assumes optically thick continuous outflows like stellar winds, and one key question arises: how is the wind-launched radius connected to physical processes in TDEs? Here we propose one possibility: through a comparison between the escape velocities estimated from their black hole masses and the wind velocities estimated from observed line widths, the outflow is launched from the self-interaction radius ($R_{\rm SI}$) where the stellar debris stretched by the tidal force intersects. We show that the escape velocities at $R_{\rm SI}$ are roughly consistent with the wind velocities. By applying the model to a sample of optical/UV TDE candidates, we find that explosive mass ejections ($\gtrsim 10\,M_{\odot}\,{\rm yr}^{-1}$) from $R_{\rm SI}$ ($\sim 10^{14}$ cm) can explain the observed properties of TDEs around peak luminosity. We also apply the same framework to a peculiar transient, AT2018cow. This model suggests that AT2018cow is likely a TDE induced by an intermediate-mass black hole ($M_{\rm BH} \sim 10^4\,M_{\odot}$).

Unified Astronomy Thesaurus concepts: Transient sources (1851); Tidal disruption (1696); Stellar winds (1636)

1. Introduction

When a star approaches a supermassive black hole (SMBH) into its tidal radius, the tidal force of the SMBH destroys the star. This phenomenon is known as a tidal disruption event (TDE). In the TDE, roughly half of the stellar debris is bound and then accreted onto the SMBH, while the rest is unbound and escapes the system (Rees 1988). As a result, the system is believed to release a large amount of energy to power a bright transient for a relatively brief time ($\lesssim$1 yr).

In the classical picture, the accretion power is the main energy source of TDEs (Komossa 2002). The luminosity increases rapidly toward the peak, and then decreases with a power law, described as $L \propto t^{-5/3}$ (Phinney 1989). The model predicts that the TDE has a peak in the radiation energy around the soft X-rays. Indeed, the first TDE candidate was discovered by ROSAT (Donley et al. 2002). However, in recent years, new-generation surveys such as the Panoramic Survey Telescope and Rapid Response System (Pan-STARRS; Kaiser et al. 2002), the Palomar Transient Factory (PTF; Law et al. 2009), the All-Sky Automated Survey for SuperNovae (ASAS-SN; Shappee et al. 2014), and the Zwicky Transient Facility (ZTF; Bellm et al. 2019), have discovered TDEs that are bright in the optical/ultraviolet (UV) wavelengths.

Typical features of optical/UV TDEs include a high peak bolometric luminosity ($L_{\rm peak} \sim 10^{44}\,{\rm erg\,s^{-1}}$), a high blackbody temperature at a few $\times\ 10^4$ K, a blue continuum component, and broad spectral lines of H, He, and N corresponding to the velocity of $\sim 10^4\,{\rm km\,s^{-1}}$ (Arcavi et al. 2014; van Velzen et al. 2020). These features may depend on the physical properties of a disrupted star (e.g., MacLeod et al. 2012), a behavior of a stream stretched by the tidal force (e.g., Strubbe & Quataert 2009), radiative transfer effects (e.g., Roth & Kasen 2018), or other factors.

In recent years, it has been suspected that optically thick outflows of the stellar debris form the optical/UV photosphere (Strubbe & Quataert 2009; Metzger & Stone 2016), and that the direct radiation from the disk is observable only in the late phase. Some models have proposed that the origin of the outflows could be super-Eddington winds (Strubbe & Quataert 2009; Lodato & Rossi 2011) or the stream-collision outflow (Jiang et al. 2016; Lu & Bonnerot 2020). However, the details still remain unclear.

In this study, by applying the "wind-driven model" (Uno & Maeda 2020) to a sample of optical/UV TDE candidates, we aim to understand the origin of the optical/UV radiation. This model assumes optically thick continuous outflows characterized by the mass-loss rate ($\dot{M}$) and the wind velocity, which are analogous to stellar winds. We note that similar models have been proposed for the optical/UV TDEs (e.g., Piro & Lu 2020), but so far the models have not been applied to a sample of observed TDEs (but see Matsumoto & Piran 2020). For example, in this Letter we show that the winds are likely to be launched from the self-interaction radii ($R_{\rm SI}$, e.g., Piran et al. 2015; Dai et al. 2015), through the comparison between escape velocities ($v_{\rm esc}$) and wind velocities ($v_{\rm wind}$). The radius is one of the characteristic radii of TDEs, in which the stellar debris stream stretched by the tidal force intersects. We further estimate the mass-loss rates of these TDEs at their peak luminosity and discuss the physical properties of the disrupted stars.

This Letter is structured as follows. In Section 2, we introduce observational properties of the sample of TDEs. In Section 3, we apply the wind-driven model to these observed TDEs and compute their $R_{\rm SI}$. We also estimate the peak mass-loss rate ($\dot{M}_{\rm peak}$) for each TDE. We then apply the same framework to a peculiar transient, AT2018cow, and discuss its origin in Section 4. Conclusions are presented in Section 5.

2. The Properties of 21 TDEs

Here we introduce some observational properties of the optical/UV TDE candidates. We select the candidates discovered by surveys such as PTF, ASAS-SN, and ZTF. To

Table 1
Sample of 21 TDE Candidates

Object	$\log_{10} M_{\rm BH}$ ($M_\odot$)	$\log_{10} L_{\rm peak}$ (erg s^{-1})	$T_{\rm peak}$ (10^4 K)	Spectral Type	FWHM (km s^{-1})	FWHM line(Å)	FWHM (day)	$L/L_{\rm edd}$	References	$R_{\rm SI}$ (10^{14} cm)
TDE2	$7.00^{+0.30}_{-0.30}$	>43.6	1.8	TDE-H	8000	Hα	⋯	0.032	a	2.62
PTF09ge	$6.31^{+0.39}_{-0.39}$	44.1	2.2	TDE-He	10100	He II(4686)	−1	0.74	b,c	6.15
PTF09axc	$5.68^{+0.48}_{-0.49}$	43.5	1.2	TDE-H	11900	Hα	+7	0.50	b,c	3.94
PTF09djl	$5.82^{+0.56}_{-0.58}$	43.9	2.6	TDE-H	6530	Hα	+2	0.93	b,c	4.67
PS1-10jh	$5.85^{+0.44}_{-0.44}$	44.5	2.9	TDE-He	9000	He II(4686)	<0	3.1	d,c,e	4.82
PS1-11af	$6.90^{+0.10}_{-0.12}$	43.9	1.5	⋯	10200	Mg II(2680)	+24	0.082	f,e	3.14
ASASSN-14ae	$5.42^{+0.46}_{-0.46}$	43.9	2.2	TDE-H	17000	Hα	+3	2.4	g,c,e	2.75
ASSASN-14li	$6.23^{+0.39}_{-0.40}$	43.8	3.5	TDE-Bowen	3000	Hα	+10	0.29	h,c,e	6.17
ASASSN-15lh	$8.88^{+0.60}_{-0.60}$	45.3	2.1	⋯	7300	4200	⋯	0.020	i	0.887
ASASSN-15oi	$6.40^{+0.54}_{-0.55}$	43.1	2.0	TDE-He	20000	He II(4686)	+7	0.57	j,e	5.97
iPTF15af	$6.88^{+0.38}_{-0.38}$	44.2	4.9	TDE-Bowen	11000	He II(4686)	+7	0.15	k,c	3.28
iPTF16axa	$6.34^{+0.42}_{-0.42}$	44.0	3.0	TDE-Bowen	8800	Hα	+6	0.38	l,c,e	6.11
iPTF16fnl	$5.50^{+0.42}_{-0.42}$	43.0	2.1	TDE-Bowen	10000	Hα	0	0.24	m,c,e	3.09
AT2017eqx	$6.77^{+0.17}_{-0.18}$	44.6	2.1	TDE-Bowen	19000	Hα	+11	0.43	n,e	3.94
PS18kh	$6.90^{+0.29}_{-0.30}$	43.9	1.5	TDE-H	11500	Hα	+6	0.085	o,e	3.16
ASASSN-18jd	$7.60^{+0.40}_{-0.40}$	44.7	2.9	TDE-Bowen	3250	Hα	average	0.087	p	0.782
ASASSN-18pg	$6.99^{+0.23}_{-0.23}$	44.4	3.1	TDE-Bowen	15000	Hα	⋯	0.17	q,e	2.67
AT2018hyz	$6.09^{+0.30}_{-0.30}$	44.3	2.2	TDE-H	17000	Hα	peak	1.2	r,e	5.89
ASASSN-19bt	$6.78^{+0.26}_{-0.26}$	44.1	1.9	TDE-H	27000	Hα	+8	0.15	s,e	3.89
ASASSN-19dj	$7.10^{+0.22}_{-0.22}$	44.8	4.5	TDE-Bowen	17000	Hα	⋯	0.38	t,e	2.17
AT2019qiz	$5.75^{+0.45}_{-0.45}$	43.7	1.9	TDE-Bowen	15000	Hα	⋯	0.64	u,e	4.30

Note. We show the observed properties ($M_{\rm BH}$, $L_{\rm peak}$, $T_{\rm peak}$, and FWHM) for a sample of 21 TDEs studied in this Letter. The spectral type refers to van Velzen et al. (2020). In the eighth column, we list the date when their FWHM was observed after peak luminosity. We calculate $R_{\rm SI}$ assuming $R_* = R_\odot$, $M_* = M_\odot$, and $\beta = 1$ (see the main text in Section 3.1).

References. a: van Velzen et al. (2011), b: Arcavi et al. (2014), c: Wevers et al. (2017), d: Gezari et al. (2012), e: Hinkle et al. (2020), f: Chornock et al. (2014), g: Holoien et al. (2014), h: Holoien et al. (2016a), i: Leloudas et al. (2016), j: Holoien et al. (2016b), k: Blagorodnova et al. (2019), l: Hung et al. (2017), m: Blagorodnova et al. (2017), n: Nicholl et al. (2019), o: Holoien et al. (2019a), p: Neustadt et al. (2020), q: Holoien et al. (2020), r: Short et al. (2020), s: Holoien et al. (2019b), t: Hinkle et al. (2021), u: Nicholl et al. (2020).

obtain unique solutions using the wind-driven model, we need to select TDEs with sufficient information. The requirements are as follows: (1) the black hole (BH) mass ($M_{\rm BH}$) has been estimated using the $M_{\rm BH}$–σ relation or the $M_{\rm bulge}$–$M_{\rm BH}$ relation (Kormendy & Ho 2013; McConnell & Ma 2013), (2) the peak luminosity and temperature have been obtained, and (3) the spectral line widths have been derived around the peak luminosity. We select 21 Optical/UV TDEs that satisfy the above criteria, and summarize their observational properties in Table 1.

In Table 1, we present the classification based on the observed spectra presented in van Velzen et al. (2020); TDE-H, TDE-Bowen, and TDE-He. We also show the FWHM of a selected line. We use the FWHM as their $v_{\rm wind}$. We use Hα for objects where Hα is observed, i.e., TDE-H and TDE-Bowen, and He II for those where Hα is not observed, i.e., TDE-He. PS1-11af has featureless spectral lines and we cannot identify the spectral lines. We also do not identify the classification of ASASSN-15lh. For $v_{\rm wind}$ of PS1-11af, we use the spectral line width around 2680Å, which is presumed to be Mg II (Chornock et al. 2014). We use the width of the main feature at 4200Å for $v_{\rm wind}$ of ASASSN-15lh (Leloudas et al. 2016).

3. Wind-driven Model for a Sample of TDEs

In some models, it is believed that optically thick flares or outflows originated in stellar debris form in the optical/UV photosphere and emission and/or absorption in their spectral lines (Strubbe & Quataert 2009; Metzger & Stone 2016; Lu & Bonnerot 2020; Piro & Lu 2020). Here, we consider the wind-driven model by Uno & Maeda (2020) to test whether continuous outflows can explain the properties of the optical/UV TDEs.

We apply the wind-driven model to the sample of the 21 TDE candidates. By applying the model, we can estimate some physical properties (the mass-loss rates and some physical scales) from observational properties (luminosity, temperature, and wind velocities). The model defines the innermost radius ($R_{\rm eq}$) where the wind is launched. In the original formalism, it is assumed that equipartition is realized between the internal energy (dominated by radiation) and the kinetic energy. However, in this Letter, we follow an inverse approach; first we assume $R_{\rm eq} = R_{\rm SI}$, and then we test whether the equipartition is indeed realized there. This way, we will show that this assumption is supported by TDE observations.

3.1. The Assumption: $R_{eq} = R_{SI}$

$R_{\rm SI}$ depends on the physical properties of the BH and the disrupted star. It is described by Dai et al. (2015) and Wevers et al. (2017) as follows:

$$R_{\rm SI} = \frac{R_{\rm t}(1+e)}{\beta(1 - e\cos(\delta\omega/2))}, \quad (1)$$

where $R_{\rm t}$ is the tidal radius given as $R_{\rm t} \approx R_*(M_{\rm BH}/M_*)^{1/3}$, where R_* and M_* are the radius and mass of the disrupted star.

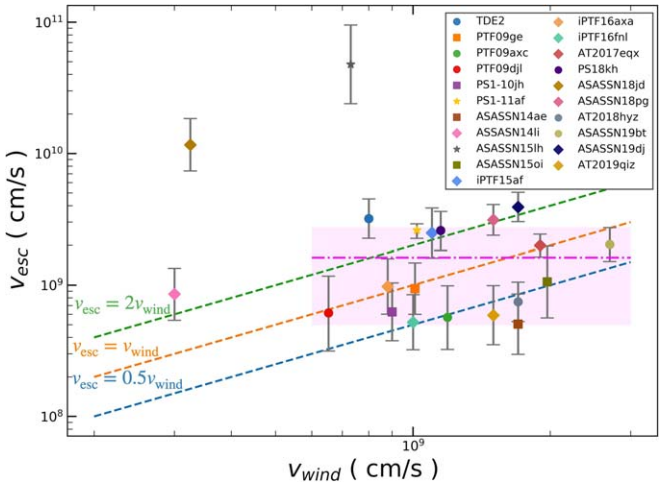

Figure 1. Comparison between $v_{\rm wind}$ and $v_{\rm esc}$. The symbols are different for different spectral types of TDEs (van Velzen et al. 2020). The filled circles, diamonds, squares, and stars show TDE-H, TDE-Bowen, TDE-He, and unspecified spectral type, respectively. The blue, orange, and green dashed lines show $v_{\rm esc} = 0.5v_{\rm wind}$, $v_{\rm esc} = v_{\rm wind}$, and $v_{\rm esc} = 2v_{\rm wind}$, respectively. The magenta dashed–dotted line shows the mean value of $v_{\rm esc}$ of the sample, excluding ASASSN-15lh, ASASSN-18jd, and ASASSN-14li (see the main text). The region enclosed by magenta shows the 1-sigma region ($\mu - \sigma \leqslant v_{\rm esc} \leqslant \mu + \sigma$).

The impact parameter is given as $\beta = R_{\rm t}/R_{\rm p}$, where $R_{\rm p}$ is the pericenter distance. e is the orbital eccentricity. $\delta\,\omega$ is given by Wevers et al. (2017) as follows:

$$\delta\omega = A_{\rm S} - 2A_{\rm J}\cos(i), \tag{2}$$

where i is the inclination. $A_{\rm S}$ and $A_{\rm J}$ are given by Merritt et al. (2010) as follows:

$$A_{\rm S} = \frac{6\pi}{c^2}\frac{GM_{\rm BH}}{R_{\rm p}(1+e)}, \quad \text{and} \tag{3}$$

$$A_{\rm J} = \frac{4\pi a_{\rm BH}}{c^3}\left(\frac{GM_{\rm BH}}{R_{\rm p}(1+e)}\right)^{3/2}, \tag{4}$$

where c, G, and $a_{\rm BH}$ are the light speed, the Newtonian constant of gravitation, and the BH spin, respectively.

For TDEs, the condition $\beta \gtrsim 1$ needs to be satisfied. In this study, we assume $\beta = 1$. This assumption is appropriate in comparing the model with the observations, as $\beta = 1$ means a large collision cross section, i.e., a high event rate. In addition, a low β, i.e., a low angular momentum, is likely preferred to produce low-energy radiation such as the optical/UV wavelengths (e.g., see Dai et al. 2015). We also assume that the radii and masses of the disrupted stars are $R_* = R_\odot$ and $M_* = M_\odot$. This assumption would be acceptable, as main-sequence stars like the Sun are most likely to be destroyed after their abundance. Under these assumptions, we compute $R_{\rm SI}$ as shown in Table 1.

To test the assumption, $R_{\rm eq} = R_{\rm SI}$, we estimate $v_{\rm esc}$ at $R_{\rm SI}$, using $v_{\rm esc} = \sqrt{2GM_{\rm BH}/R_{\rm SI}}$. We regard the FWHM as $v_{\rm wind}$, and show the comparison between $v_{\rm esc}$ and $v_{\rm wind}$ in Figure 1. Figure 1 shows that $v_{\rm esc}$ is roughly consistent with $v_{\rm wind}$ within a factor of 2. However, discussing this possible correlation any further is difficult, as accurately deriving $v_{\rm wind}$ from observational data involves a large uncertainty. In addition, the present sample for this analysis remains limited. Indeed, the values of $v_{\rm wind}$ of most of the TDE samples here fall into a limited range within a factor of 3 (except for ASASSN-15lh, ASASSN-18jd, and ASASSN-14li, in which the former two are outliers). Therefore, the present sample would not allow such a detailed investigation of the correlation; the correlation coefficient between $v_{\rm esc}$ and $v_{\rm wind}$ is indeed smaller than 0.2, but this may simply be an outcome of the currently limited samples. Alternatively, we may simply discuss the mean and standard deviation in the distribution of $v_{\rm esc}$ (excluding the above mentioned three objects). The mean and standard deviation are $\mu = 1.62 \times 10^9\,{\rm cm\,s^{-1}}$ and $\sigma = 1.12 \times 10^9\,{\rm cm\,s^{-1}}$, respectively. This is roughly consistent with the above estimate within a factor of 2. In the future, we hope to analyze the possible correlation further, once the sufficiently large sample covering a range of $v_{\rm wind}$ becomes available and the relation between $v_{\rm wind}$ and the observed line width is better clarified.

In the two outliers, ASASSN-15lh and ASASSN-18jd, $v_{\rm wind}$ is significantly lower than $v_{\rm esc}$. This suggests that these objects are beyond the applicability of this model. Indeed, the observations show that ASASSN-15lh may be induced by an SMBH with mass above the upper limit to produce TDEs ($\sim 10^8\,M_\odot$). ASASSN-18jd is not robustly identified as a TDE; we cannot dismiss the possibility that ASASSN-18jd is an active galactic nucleus or an unknown type of transient. We may need to consider different scenarios or emission mechanisms for these objects, including a possibility of a high BH spin (Mummery & Balbus 2020, see also Section 4).

In Figure 1, different spectral types of TDEs (van Velzen et al. 2020) are shown by different symbols. No clear difference is seen in the distribution of $v_{\rm esc}$ and $v_{\rm wind}$ for different spectral types.

3.2. Estimate of Physical Properties

In Uno & Maeda (2020), $R_{\rm eq}$ was one of the output parameters. However, in the present work, we treat $R_{\rm eq}$ as an input parameter under the assumption $R_{\rm eq} = R_{\rm SI}$. We alternately introduce a new parameter, f, into the equations. The new parameter f is the ratio of the kinetic energy ($\varepsilon_{\rm kin}$) to the thermal energy ($\varepsilon_{\rm th}$) per unit of volume at $R_{\rm SI}$. f is described as $f = \varepsilon_{\rm th}/\varepsilon_{\rm kin}$. In Uno & Maeda (2020) it is assumed that $\varepsilon_{\rm th} = \varepsilon_{\rm kin}$ holds at $R_{\rm eq}$, but this time we incorporate the ratio as a new unknown parameter. We expect that the derived value of f should be an order of unity, if the model is self-consistent.

Uno & Maeda (2020) defines three typical physical scales: the wind-launched radius ($R_{\rm eq}$), the photon-trapped radius ($R_{\rm ad}$), and the color radius ($R_{\rm c}$). In this study, we replace $R_{\rm eq}$ by $R_{\rm SI}$. At $R_{\rm SI}$, we assume the following relation:

$$aT(R_{\rm SI})^4 = f\frac{1}{2}\rho(R_{\rm SI})v^2, \tag{5}$$

where the density structure, $\rho(r)$, is given as follows:

$$\rho(r) = \frac{\dot{M}}{4\pi r^2 v}. \tag{6}$$

We assume that $v_{\rm wind}$ is constant as a function of radius. $R_{\rm ad}$ is defined by $\tau_{\rm s}(R_{\rm ad}) = c/v$, where $\tau_{\rm s}$ is the optical depth for electron scattering. $R_{\rm c}$ is defined by $\tau_{\rm eff}(R_{\rm c}) = 1$, where $\tau_{\rm eff}$ is the effective optical depth, considering not only electron scattering but also absorption processes. The formation of the photosphere depends on a relative relation between $R_{\rm c}$ and $R_{\rm ad}$. The photospheric radius ($R_{\rm ph}$) is given as $R_{\rm ph} = \max(R_{\rm ad}, R_{\rm c})$.

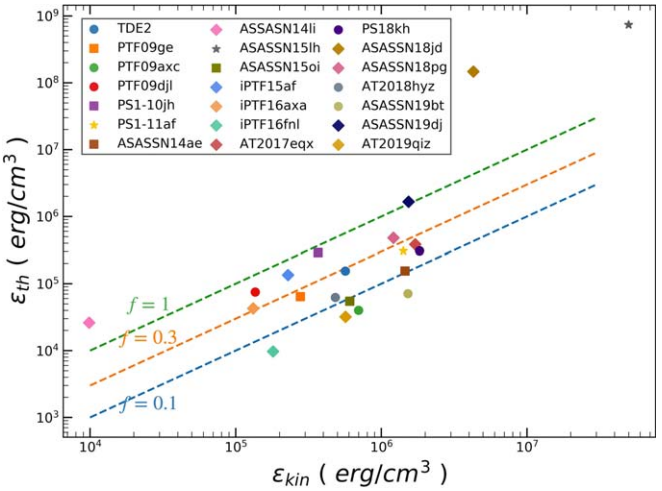

Figure 2. Comparison between $\varepsilon_{\rm kin}$ and $\varepsilon_{\rm th}$. The blue, orange, and green dashed lines show $f = 0.1$, $f = 0.3$, and $f = 1$, respectively.

We also define the luminosity as follows:

$$L(r) = -\frac{4\pi r^2 ac}{3\kappa_{\rm s}\rho}\frac{\partial}{\partial r}T^4. \quad (7)$$

Using above equations, we can estimate f and $\dot{M}$. When $R_{\rm c} < R_{\rm ad}$, they are given as follows:

$$\dot{M} \approx 21\, M_\odot\ {\rm yr}^{-1}\left(\frac{L}{1.0\times10^{44}\ {\rm erg\ s^{-1}}}\right)^{\frac{1}{2}} \times\left(\frac{T_{\rm ph}}{3.0\times10^4\ {\rm K}}\right)^{-2}\left(\frac{v}{9.0\times10^8\ {\rm cm\ s^{-1}}}\right)^{-\frac{1}{2}}, \text{ and} \quad (8)$$

$$f \approx 0.29\left(\frac{L}{1.0\times10^{44}\ {\rm erg\ s^{-1}}}\right)^{\frac{5}{6}}\left(\frac{T_{\rm ph}}{3.0\times10^4\ {\rm K}}\right)^{\frac{2}{3}} \times\left(\frac{v}{9.0\times10^8\ {\rm cm\ s^{-1}}}\right)^{-\frac{11}{6}}\left(\frac{R_{\rm SI}}{6.0\times10^{14}\ {\rm cm}}\right)^{-\frac{2}{3}}, \quad (9)$$

where $T_{\rm ph}$ is the photospheric temperature; $T_{\rm ph} = T(R_{\rm ph})$. On the other hand, if $R_{\rm c} > R_{\rm ad}$ holds, the parameters are given as follows:

$$\dot{M} \approx 19\, M_\odot\ {\rm yr}^{-1}\left(\frac{L}{8.0\times10^{43}\ {\rm erg\ s^{-1}}}\right)^{\frac{4}{5}} \times\left(\frac{T_{\rm ph}}{2.5\times10^4\ {\rm K}}\right)^{-\frac{11}{10}}\left(\frac{v}{6.5\times10^8\ {\rm cm\ s^{-1}}}\right), \text{ and} \quad (10)$$

$$f \approx 0.53\left(\frac{L}{8.0\times10^{43}\ {\rm erg\ s^{-1}}}\right)^{\frac{11}{15}}\left(\frac{T_{\rm ph}}{2.5\times10^4\ {\rm K}}\right)^{\frac{11}{30}} \times\left(\frac{v}{6.5\times10^8\ {\rm cm\ s^{-1}}}\right)^{-\frac{7}{3}}\left(\frac{R_{\rm SI}}{5.0\times10^{14}\ {\rm cm}}\right)^{-\frac{2}{3}}. \quad (11)$$

Figure 2 shows the comparison between $\varepsilon_{\rm kin}$ and $\varepsilon_{\rm th}$ as we have derived it. This shows a roughly positive correlation, but there are two objects which are clearly out of the trend; ASASSN-15lh and ASASSN-18jd. These are also the outliers in Figure 1. This also suggests that they are beyond the applicability of the present model. Generally, the outflow may well be launched from a radius where $\varepsilon_{\rm kin}$ and $\varepsilon_{\rm th}$ become comparable, i.e., $f \sim 1$ (Strubbe & Quataert 2009). Except for the two outliers, the ratio roughly stays in the range between 0.1 and 1. We suggest that this result is another strong support for $R_{\rm eq} = R_{\rm SI}$.

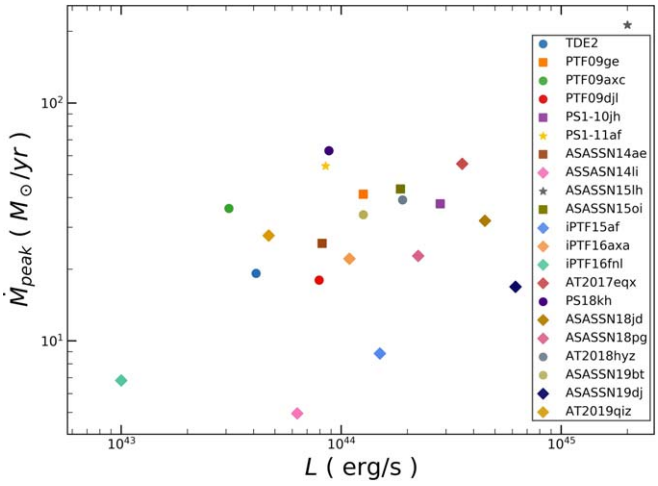

Figure 3. $\dot{M}_{\rm peak}$ estimated by the wind-driven model.

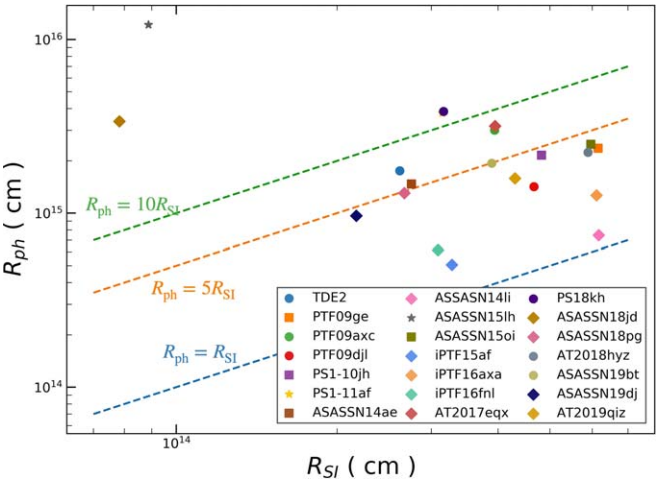

Figure 4. Comparison between $R_{\rm SI}$ and $R_{\rm ph}$. The blue, orange, and green dashed lines show $R_{\rm ph} = R_{\rm SI}$, $R_{\rm ph} = 5R_{\rm SI}$, and $R_{\rm ph} = 10R_{\rm SI}$, respectively.

Figure 3 shows the estimated $\dot{M}_{\rm peak}$. We find that TDEs have strong outflows around the peak luminosity, typically with $\dot{M}_{\rm peak} \gtrsim 10\, M_\odot\ {\rm yr}^{-1}$. Assuming that the disrupted star is $M_* \sim M_\odot$, they cannot release the mass exceeding $\sim 1\, M_\odot$. Extremely large mass-loss rates (e.g., ASASSN-15lh) are not feasible. This is another important constraint to identify the limits in the application of the model (see also Section 4).

Figure 4 shows the comparison between $R_{\rm SI}$ and $R_{\rm ph}$. Typically, $R_{\rm ph}$ is formed above $R_{\rm SI}$, between $\sim R_{\rm SI}$ and $\sim 10R_{\rm SI}$. This result supports the picture that the origin of the optical/UV radiation and some spectral lines is not the direct radiation from the accretion disk, but is the optically thick winds (Strubbe & Quataert 2009).

4. Discussion

We have generally derived high mass-loss rates for a sample of TDEs as an outcome of the wind-driven model for TDEs. Indeed, TDEs are expected to have high accretion rates at peak. In Stone et al. (2013) the peak fall-back rate, described as $\dot{M}_{\rm fb}$,

is roughly given as follows:

$$\frac{\dot{M}_{\rm fb}}{\dot{M}_{\rm Edd}} \approx 133\left(\frac{\eta}{0.1}\right)\left(\frac{M_{\rm BH}}{10^6 M_\odot}\right)^{-\frac{3}{2}}\left(\frac{M_*}{M_\odot}\right)^{\frac{4}{5}}, \quad (12)$$

where $\dot{M}_{\rm Edd} = 4\pi G M_{\rm BH}/(\kappa_{\rm s}\eta c)$, or,

$$\dot{M}_{\rm fb} \approx 3.45\, M_\odot\ {\rm yr}^{-1}\left(\frac{M_{\rm BH}}{10^6 M_\odot}\right)^{-\frac{1}{2}}\left(\frac{M_*}{M_\odot}\right)^{\frac{4}{5}}. \quad (13)$$

Because this is the super-Eddington accretion, it is likely that most of the accretion may be ejected (i.e., outflows), and therefore the accretion rate here may represent the mass-loss rate. Therefore, the high mass-loss rate that we derived is in line with this expectation from the TDE physics. While it is true that the theoretically expected rate here is a few times smaller than our estimate, we note that both estimates involve uncertainties that would not allow detailed comparison.

Because TDEs are highly time-dependent transients, further discussion requires the effect of time evolution (see, e.g., Uno & Maeda 2020). One way to take this into account is to check the total mass ejected by the outflow. The timescale in the TDE light curve may differ from one object to another; some TDEs rapidly fade in ∼20 days, while others stay bright for about a year (van Velzen et al. 2020). With this caveat in mind, we adopt one month as the typical timescale, as most TDEs typically fade substantially in this timescale. By multiplying this timescale to the peak luminosities, the total ejected masses are expected to be a few $M_\odot$ (see also Figure 3).

Because we assume $M_* = M_\odot$, the system cannot eject mass larger than $M_\odot$. However, $R_{\rm SI}$, which affects the mass-loss rates, depends on M_* as follows: $R_{\rm SI} \propto R_{\rm t} \propto R_* M_*^{-1/3}$. For larger disrupted stars, we thus expect that $R_{\rm SI}$ roughly stays the same because both R_* and M_* become larger. Therefore, considering more massive stars would not alter the present results substantially, and therefore the mass ejection of a few $M_\odot$ can be easily accommodated.

Indeed, Matsumoto & Piran (2020) have recently estimated the mass ejection of some TDEs using the model similar to the present work. They have applied the model to a few TDEs, partially taking time evolution into account. They thereby derived $\sim 10\, M_\odot$ for the total ejected mass. This is roughly consistent with our estimate. With this value, they indeed have argued against the wind-driven model for TDEs. However, given that both models still lack detailed treatment of time evolution and also use some simplified assumptions (e.g., treatment of opacity), and that we find a few other independent supports for the wind-driven model, we do take this rough agreement in the ejected mass between our estimate and the TDE expectation as another support for the applicability of the wind-driven model to TDEs.

As mentioned above, further detailed analysis will require the full time-dependent treatment. Before being able to sophisticate the model at this level, we indeed need to overcome several limitations in our current understanding of the observational data of TDEs. For example, our current understanding of the evolution of $v_{\rm wind}$ is not sufficient, which requires deeper understanding of the line-formation processes (see, e.g., Uno & Maeda 2020). Also, a sample of TDEs with well-sampled time-evolution data is still limited. Therefore, in this work, we focus on the properties of TDEs at their peaks, aiming at understanding the general/statistical properties of TDEs using as large an observed sample as is currently available. In the future, we hope to address the time-evolution effects and apply such a model to a sample of TDEs with the time-evolution data available, but this is beyond the scope of the present work.

Mummery & Balbus (2020) presented ASASSN-15lh as a peculiar TDE that has a high BH spin close to $a_{\rm BH} \approx 0.99$. Adopting the high BH spin, we applied our model to ASASSN-15lh. The main change is seen in the value of f, but this is only about 2%. Taking into account the fact that the BH spin does not have a significant effect on the derived properties based on the wind model, e.g., mass-loss rate. ASASSN-15lh thus remains an outlier, which seems to be beyond the applicability of our present model.

Using the wind-driven model and results, we can obtain insights for TDEs or other astronomical transients driven by explosive mass ejection. Namely, we can constrain some physical properties for transients with insufficient observational data. For example, we can roughly estimate $M_{\rm BH}$ or $v_{\rm wind}$.

As one example of such an application, we estimate $M_{\rm BH}$ for a peculiar transient, AT2018cow (Prentice et al. 2018). AT2018cow is a luminous blue transient ($L_{\rm peak} \approx 4 \times 10^{44}\,{\rm erg\,s^{-1}}$, $T_{\rm peak} \approx 31{,}400\,{\rm K}$, and $v \approx 0.1c$) discovered by ATLAS on MJD 58285 (Perley et al. 2019). Perley et al. (2019) argued that AT2018cow is a TDE induced by an intermediate-mass black hole (IMBH). However, AT2018cow occurred far from the galactic center, which makes it difficult to estimate $M_{\rm BH}$ from the $M_{\rm bulge}$–$M_{\rm BH}$ relation. They estimated $M_{\rm BH}$ using Mosfit TDE model (Guillochon et al. 2018). In our model, we can constrain $M_{\rm BH}$ independently from Mosfit. Assuming $R_* = R_\odot$, $M_* = M_\odot$, $\beta = 1$, and $f = 0.5$, we estimate $M_{\rm BH}$ as $\sim 2.5 \times 10^4\, M_\odot$. This is consistent with the estimate by Perley et al. (2019). Our model thus supports the hypothesis that AT2018cow may be a TDE induced by an IMBH. In addition, we note that $R_{\rm SI}$ estimated by Perley et al. (2019) is a factor of 10 smaller than the observed photosphere. This is also consistent with our result (see Figure 4), supporting by the wind-driven model.

5. Conclusions

Using the wind-driven model presented by Uno & Maeda (2020), we have aimed to constrain the origin of the optical/UV radiation in TDEs. The comparison between the escape velocities and the wind velocities supports the hypothesis that the wind is launched from the self-interaction radius. Generally, the wind is expected to be launched from a position where the ratio of kinetic to thermal energy per unit volume is roughly equal (i.e., equipartition). We also estimate the ratio at the self-interaction radius through the wind-driven model, and it turns out to be an order of unity. This result supports the assumption that the stream collision induces the wind.

We find TDEs have strong outflow around the peak. The mass-loss rates are typically over $10\, M_\odot\,{\rm yr}^{-1}$. We also show that the photospheric radii are 1–10 times larger than the self-interaction radii. This result supports the picture that the optical/UV radiation is emitted not from the accretion disk directly, but from an optically thick wind.

By applying the framework to TDEs or other astronomical transients driven by explosive mass ejections, we can obtain constraints on the physical properties that cannot be obtained from observations. We apply the framework to a peculiar

transient, AT2018cow. The model suggests that AT2018cow is likely a TDE induced by an IMBH ($\sim 10^4\,M_\odot$).

The wind-driven model still has significant room for improvement. The present model assumes a steady-state, and in this Letter we estimate physical quantities only at the peak. To obtain detailed constraints, it is necessary to create a non-steady-state model that takes into account the time evolution and radial dependence of the velocity. We leave such work to future studies.

We thank Girogs Leloudas and Tatsuya Matsumoto for helpful comments and discussions. K.M. acknowledges support provided by Japan Society for the Promotion of Science (JSPS) through KAKENHI grant (JP18H05223, JP20H00174, and JP20H04737).

ORCID iDs

Kohki Uno https://orcid.org/0000-0002-6765-8988
Keiichi Maeda https://orcid.org/0000-0003-2611-7269

References

Arcavi, I., Gal-Yam, A., Sullivan, M., et al. 2014, ApJ, 793, 38
Bellm, E. C., Kulkarni, S. R., Graham, M. J., et al. 2019, PASP, 131, 018002
Blagorodnova, N., Cenko, S. B., Kulkarni, S. R., et al. 2019, ApJ, 873, 92
Blagorodnova, N., Gezari, S., Hung, T., et al. 2017, ApJ, 844, 46
Chornock, R., Berger, E., Gezari, S., et al. 2014, ApJ, 780, 44
Dai, L., McKinney, J. C., & Miller, M. C. 2015, ApJL, 812, L39
Donley, J. L., Brandt, W. N., Eracleous, M., & Boller, T. 2002, AJ, 124, 1308
Gezari, S., Chornock, R., Rest, A., et al. 2012, Natur, 485, 217
Guillochon, J., Nicholl, M., Villar, V. A., et al. 2018, ApJS, 236, 6
Hinkle, J. T., Holoien, T. W. S., Auchettl, K., et al. 2021, MNRAS, 500, 1673
Hinkle, J. T., Holoien, T. W. S., Shappee, B. J., et al. 2020, ApJL, 894, L10
Holoien, T. W. S., Auchettl, K., Tucker, M. A., et al. 2020, ApJ, 898, 161
Holoien, T. W. S., Huber, M. E., Shappee, B. J., et al. 2019a, ApJ, 880, 120
Holoien, T. W. S., Kochanek, C. S., Prieto, J. L., et al. 2016a, MNRAS, 455, 2918
Holoien, T. W. S., Kochanek, C. S., Prieto, J. L., et al. 2016b, MNRAS, 463, 3813
Holoien, T. W. S., Prieto, J. L., Bersier, D., et al. 2014, MNRAS, 445, 3263
Holoien, T. W. S., Vallely, P. J., Auchettl, K., et al. 2019b, ApJ, 883, 111
Hung, T., Gezari, S., Blagorodnova, N., et al. 2017, ApJ, 842, 29
Jiang, Y.-F., Guillochon, J., & Loeb, A. 2016, ApJ, 830, 125
Kaiser, N., Aussel, H., Burke, B. E., et al. 2002, Proc. SPIE, 4836, 154
Komossa, S. 2002, RvMA, 15, 27
Kormendy, J., & Ho, L. C. 2013, ARA&A, 51, 511
Law, N. M., Kulkarni, S. R., Dekany, R. G., et al. 2009, PASP, 121, 1395
Leloudas, G., Fraser, M., Stone, N. C., et al. 2016, NatAs, 1, 0002
Lodato, G., & Rossi, E. M. 2011, MNRAS, 410, 359
Lu, W., & Bonnerot, C. 2020, MNRAS, 492, 686
MacLeod, M., Guillochon, J., & Ramirez-Ruiz, E. 2012, ApJ, 757, 134
Matsumoto, T., & Piran, T. 2020, arXiv:2009.01240
McConnell, N. J., & Ma, C.-P. 2013, ApJ, 764, 184
Merritt, D., Alexander, T., Mikkola, S., & Will, C. M. 2010, PhRvD, 81, 062002
Metzger, B. D., & Stone, N. C. 2016, MNRAS, 461, 948
Mummery, A., & Balbus, S. A. 2020, MNRAS, 497, L13
Neustadt, J. M. M., Holoien, T. W. S., Kochanek, C. S., et al. 2020, MNRAS, 494, 2538
Nicholl, M., Blanchard, P. K., Berger, E., et al. 2019, MNRAS, 488, 1878
Nicholl, M., Wevers, T., Oates, S. R., et al. 2020, MNRAS, 499, 482
Perley, D. A., Mazzali, P. A., Yan, L., et al. 2019, MNRAS, 484, 1031
Phinney, E. S. 1989, in IAU Symp. 136, The Center of the Galaxy, ed. M. Morris (Dordrecht: Kluwer), 543
Piran, T., Svirski, G., Krolik, J., Cheng, R. M., & Shiokawa, H. 2015, ApJ, 806, 164
Piro, A. L., & Lu, W. 2020, ApJ, 894, 2
Prentice, S. J., Maguire, K., Smartt, S. J., et al. 2018, ApJL, 865, L3
Rees, M. J. 1988, Natur, 333, 523
Roth, N., & Kasen, D. 2018, ApJ, 855, 54
Shappee, B. J., Prieto, J. L., Grupe, D., et al. 2014, ApJ, 788, 48
Short, P., Nicholl, M., Lawrence, A., et al. 2020, MNRAS, 498, 4119
Stone, N., Sari, R., & Loeb, A. 2013, MNRAS, 435, 1809
Strubbe, L. E., & Quataert, E. 2009, MNRAS, 400, 2070
Uno, K., & Maeda, K. 2020, ApJ, 897, 156
van Velzen, S., Farrar, G. R., Gezari, S., et al. 2011, ApJ, 741, 73
van Velzen, S., Gezari, S., Hammerstein, E., et al. 2020, arXiv:2001.01409
Wevers, T., van Velzen, S., Jonker, P. G., et al. 2017, MNRAS, 471, 1694